Space and time reconstruction of the precessing vortex core in Francis turbine draft tube by 2D-PIV

A Favrel[1], A Müller[1], C Landry[1], K Yamamoto[1] and F Avellan[1]

[1]EPFL Laboratory for Hydraulic Machines, Avenue de Cour 33bis 1007 Lausanne, Switzerland

E-mail: arthur.favrel@epfl.ch

Abstract. Francis turbines operating at part load conditions experience the development of a high swirling flow at the runner outlet, giving rise to the development of a cavitation precessing vortex rope in the draft tube. The latter acts as an excitation source for the hydro-mechanical system and may jeopardize the system stability if resonance conditions are met. Although many aspects of the part load issue have been widely studied in the past, the accurate stability analysis of hydro-power plants remains challenging. A better understanding of the vortex rope dynamics in a wide range of operating conditions is an important step towards the prediction and the transposition of the pressure fluctuations from reduced to prototype scale. For this purpose, an investigation of the flow velocity fields at the outlet of a Francis turbine reduced scale physical model operating at part load conditions is performed by means of 2D-PIV in three different horizontal cross-sections of the draft tube cone. The measurements are performed in cavitation-free conditions for three values of discharge factor, comprised between 60% and 81% of the value at the Best Efficiency Point. The present article describes a detailed methodology to properly recover the evolution of the velocity fields during one precession cycle by means of phase averaging. The vortex circulation is computed and the vortex trajectory over one typical precession period is finally recovered for each operating point. It is notably shown that below a given value of the discharge factor, the vortex dynamics abruptly change and loose its periodicity and coherence.

1. Introduction

Francis turbines operating with a discharge lower than the nominal discharge (part load conditions) experience the development of a cavitation precessing vortex rope at the runner outlet in the draft tube. Its rotational frequency lies between 0.2 and 0.4 times the runner frequency [1]. The precession of the vortex induces pressure fluctuations at the same frequency, which can be decomposed into two different components in the draft tube cone [1, 2, 3]. The convective or asynchronous component corresponds to the rotation of the pressure pattern with the precessing vortex core in the draft tube. The second one, called synchronous component, has been identified as the result of the excitation source produced by the precession of the vortex rope in the elbow [4] and is known to propagate into the entire hydraulic system. In case of resonance, the synchronous component becomes dominant, leading to pressure and power surges [5] able to jeopardize the stability of the machine and of the electrical grid to which it is connected. As the extension of the operating range of hydro-power plants is increasingly required due to the massive penetration of intermittent energy sources into the existing electrical grid, an accurate assessment of the stability of hydro-power plants operating at part load is essential. For this purpose, one-dimensional flow models have been developed in the past decades [4, 6, 7, 8],

in which the cavitation draft tube flow is modeled by the cavitation compliance parameter [9] and the excitation source by an additional source term in the momentum equation. Recently, these parameters have been identified by using an original experimental approach in the case of Francis turbine part load conditions [10, 11]. However, the exact physical mechanisms driving the excitation source remain unclear and sparsely documented. It is for instance essential to understand how the flow discharge influences the vortex dynamics and to establish the link between the intensity of the excitation source and the draft tube flow characteristics in a wide range of operating conditions. Several contributions have already reported the investigation of the axial velocity field in the draft tube cone at both partial load [12, 13] and full load conditions [14].

The present work aims at investigating the vortex rope dynamics and structure for different values of discharge factor at part load conditions. For this purpose, the tangential flow field is investigated at the outlet of a reduced scale physical model of a Francis turbine by means of 2D-Particle Image Velocimetry (PIV) performed in three horizontal cross-sections of the draft tube cone. A particular set-up is designed in order to guarantee a proper optical access across the complex geometry of the machine. Based on phase-averaged velocity fields, the vortex parameters, such as trajectory and circulation, are finally determined.

2. Test-case

2.1. Reduced-scale model

The investigation is performed on a reduced scale physical model of a 16 blades Francis turbine with a specific speed of $\nu = 0.27$. The model is installed on a close-looped test rig of EPFL Laboratory for Hydraulic Machines (see Figure 1). The facility includes two axial double-volute pumps generating the specified head while the discharge is adjusted by the guide vanes opening.

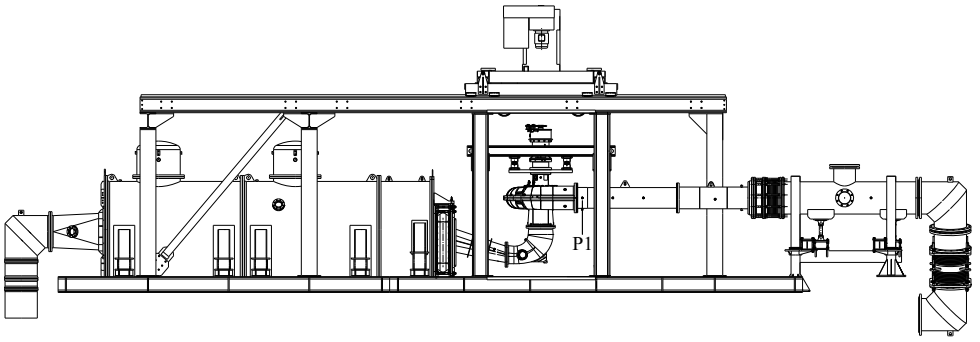

Figure 1: Reduced-scale physical model of a Francis turbine installed on EPFL test rig.

Pressure fluctuations are measured at different locations of the test-rig by flush-mounted piezo-resistive pressure sensors. In the draft tube cone, the wall pressure is measured at two different streamwise positions, respectively $0.39 \times D_{\bar{1}}$ and $1.02 \times D_{\bar{1}}$ downstream the runner outlet, $D_{\bar{1}}$ being the outer diameter of the runner. For each section, 4 pressure sensors are installed and regularly spaced by an angle of 90° (positions C1E-C1N-C1W-C1S in the upper section and positions C2E-C2N-C2W-C2S in the lower section), enabling the decomposition of the pressure fluctuations into convective and synchronous components. In the headwater connecting pipe, one pressure sensor is installed at the inlet of the spiral casing (position P1 in Figure 1).

2.2. Operating conditions

Pressure fluctuations are first performed in cavitation-free conditions in a wide range of discharge factor, from 100 % to 50 % of the value at the BEP. The speed factor is kept constant at the nominal value $n_{\mathrm{ED}} = 0.288$. The influence of the discharge factor on both the precession frequency and the amplitude of the pressure fluctuations measured in P1 is given in Figure 2.

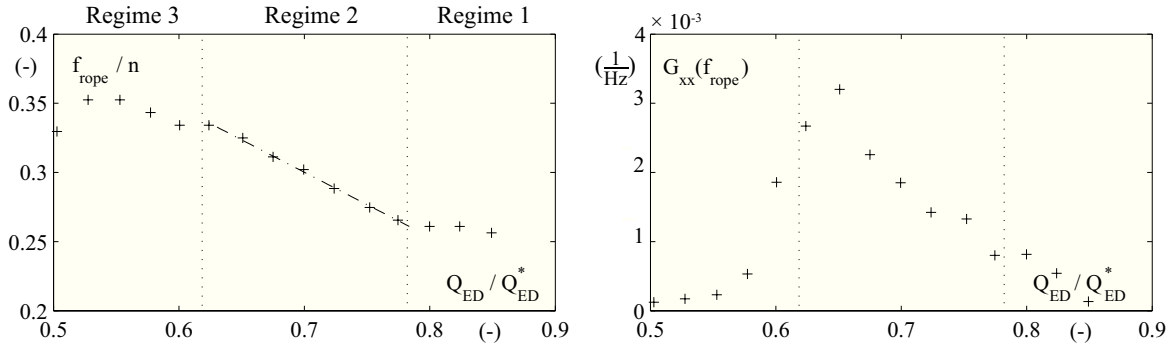

(a) Precession frequency (b) Auto-spectral amplitude at f_{rope}

Figure 2: (a) Precession frequency made dimensionless by the runner frequency and (b) auto-spectral amplitude at the precession frequency as a function of the discharge factor. The corresponding pressure signal is measured in the upstream pipe (location P1).

For each value of the discharge factor, the coherence between two pressure signals measured in the same cross-section of the cone is computed. The influence of the discharge factor on its value at the precession frequency is given in Figure 3 for two pairs of sensors.

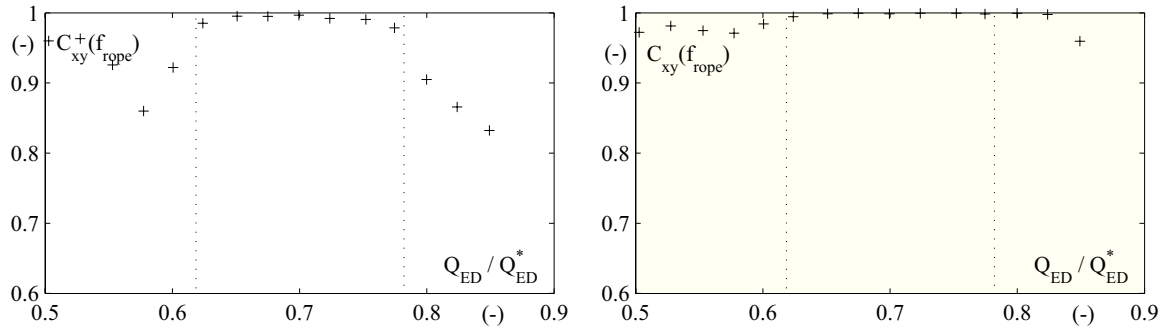

(a) Sensors C1E-C1S (b) Sensors C2E-C2S

Figure 3: Coherence at the precession frequency between two pressure signals measured in the same cone cross-section as a function of the discharge factor.

Three different flow regimes are highlighted depending on the value of the discharge factor [15]. In the flow regime 2, the precessing vortex core is highly coherent and the precession frequency linearly increases as the value of the discharge factor is decreased. The amplitude of the synchronous pressure fluctuations measured in the upstream pipe also increases and is at its maximum as the value of the discharge factor is equal to 65 % of the value at the BEP. The following study is focused on three particular operating points, corresponding to 81 %, 64 % and 60 % of the BEP. The corresponding parameters are given in Table 1.

Table 1: List of investigated operating points

OP	n_{ED}	Q_{ED}	Q_{ED}/Q^*_{ED}
1	0.288	0.161	0.81
2	0.288	0.128	0.64
3	0.288	0.120	0.60

3. PIV measurements

3.1. PIV set-up

The flow velocity fields are investigated by means of PIV in three horizontal cross-sections of the draft tube cone, situated $0.39 \times D_{\bar{1}}$, $0.75 \times D_{\bar{1}}$ and $1.02 \times D_{\bar{1}}$ downstream the runner outlet. A flat waterbow is used to minimize the optical distortion potentially induced by the curved surface of the cone. A CCD camera is placed at the bottom of the elbow and is aligned with the coordinate system of the test rig to measure directly the corresponding velocity components Cx and Cy. The set-up for the PIV measurements is presented in Figure 4. Standard 20-μm polyamide particles are used for the seeding as the measurements are performed in cavitation-free conditions.

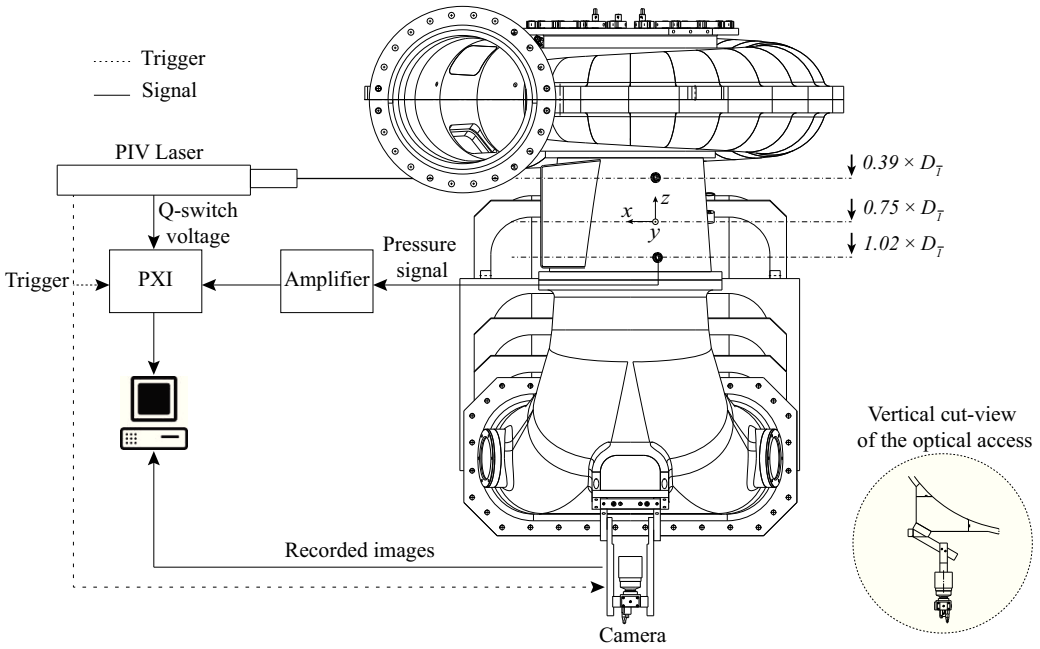

Figure 4: Experimental set-up for the PIV measurements in horizontal cross-sections of the draft tube cone, together with a cut-view of the optical access.

For each operating point, a total of 10,000 pairs of images is acquired, corresponding to 10,000 instantaneous velocity fields. In order to enable a phase averaging of the velocity fields and to recover their evolution over one precession cycle of the vortex, the output voltage of the internal trigger of the PIV system, called Q-switch, is used to determine a time stamp for each recorded instantaneous velocity field. The pairs of images are acquired continuously

with a sampling frequency of 10 Hz whereas the Q-switch voltage and the pressure signals are recorded synchronously with a sampling frequency of 1,000 Hz. An example of shortened signals is presented in Figure 5.

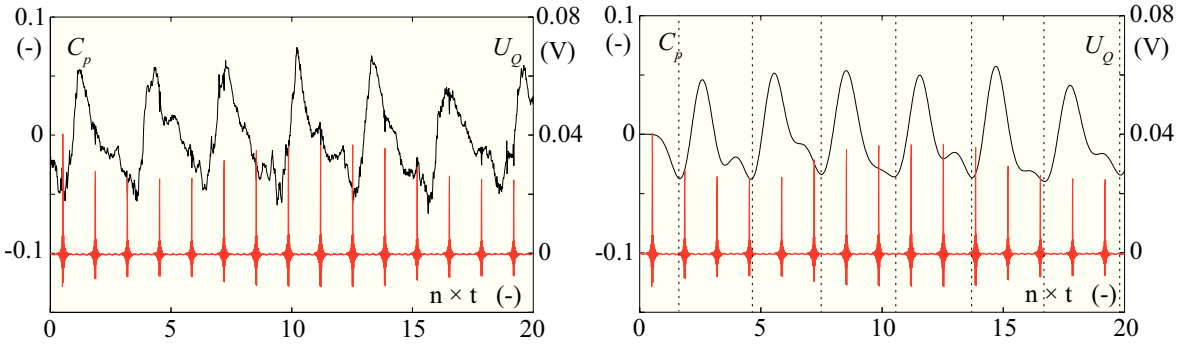

(a) Raw pressure signal

(b) Filtered pressure signal

Figure 5: Reference pressure signal (black solid line) and output voltage from Q-switch laser (red solid line). The limits of the successive precession cycles are indicated by the dashed black lines in the right-handed figure.

3.2. Post-processing methodology

Each image is first dewarped using a third-order polynomial imaging model fit based on a calibration image. Individual velocity fields are then obtained by applying an adaptive cross-correlation method to each pair of images. The resulting velocity fields contain 272×241 vectors with a spatial resolution of $\Delta x = \Delta y = 1.54$ mm, 1.63 mm and 1.68 mm in the measurement sections 1, 2, and 3, respectively.

A phase averaging of the velocity fields, based on the precession cycle identified in a reference pressure signal, is performed [16]. The different precession cycles are first determined in the reference pressure signal through their local pressure minima. Each individual precession cycle is divided into 90 phase window of 4° width. The instantaneous velocity fields measured inside the same phase window are then averaged together, resulting in 90 mean phase averaged velocity fields. They represent the periodical behaviour of the flow over one typical precession period. An example of one instantaneous velocity field and the corresponding phase averaged velocity field is given in Figure 6.

3.3. Vortex parameters

3.3.1. Vortex centre The vortex centre is determined by using the algorithm proposed by Graftieaux et al. [17], which permits to fairly identify the centre of vortical structures without computing any velocity gradient [18]. They introduced a dimensionless scalar γ_1 which is defined at a given point P by:

$$\gamma_1(P) = \frac{1}{N} \sum_{S} \frac{(\vec{PM} \wedge \vec{C}(M)) \cdot \vec{z}}{\|\vec{PM}\| \cdot \|\vec{C}(M)\|} \tag{1}$$

with S a rectangular domain of fixed size surrounding the point P, M a point inside the domain S and N the number of points inside S. The symbols $\wedge$ and $\cdot$ correspond to the cross product and the scalar product, respectively. $\vec{C}(M)$ is the velocity vector in the (x, y)-plane and $\vec{z}$ the unit vector normal to the (x, y)-plan. The vortex centre is identified as the point where

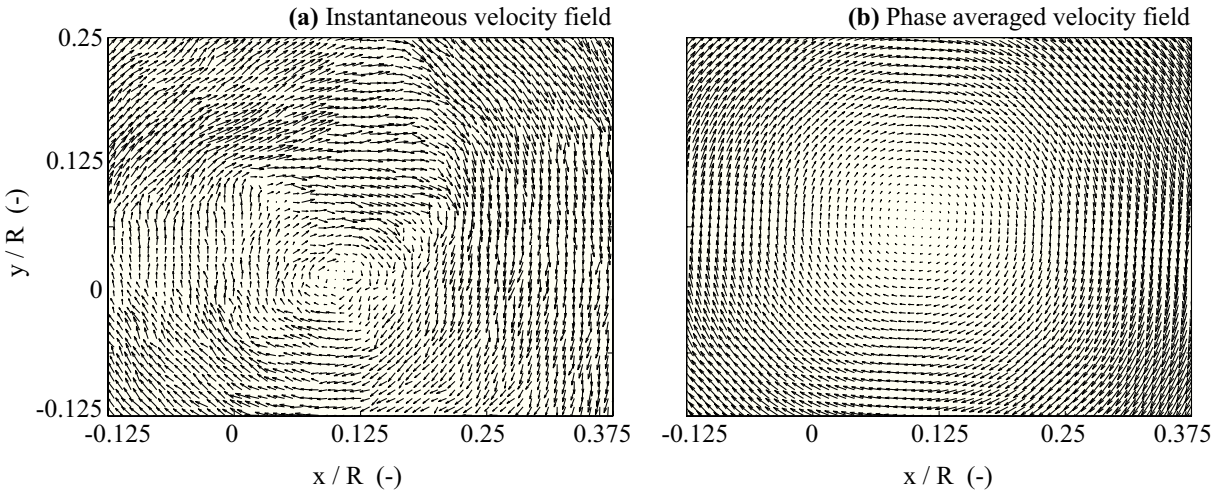

Figure 6: Example of one instantaneous velocity field, together with the corresponding phase averaged velocity field for the relative phase $\theta = 10\pi/6$ of the precession cycle.

the scalar $|\gamma_1|$ is at its maximum. In the present study, the vortex centre is identified in the phase averaged and instantaneous velocity fields, permitting to determine its average trajectory over one precession period and the corresponding dispersion.

3.3.2. Vortex circulation The vorticity $\omega_z = \frac{\partial Cy}{\partial x} - \frac{\partial Cx}{\partial y}$ is computed by direct derivation of the velocity components (Cx, Cy). The vortex circulation is then estimated by integrating the vorticity within the limits of the vortex core:

$$\Gamma = \oint_{\mathcal{C}} \vec{C} \cdot \mathrm{d}\vec{l} = \int_S \omega_z \cdot \mathrm{dS} \tag{2}$$

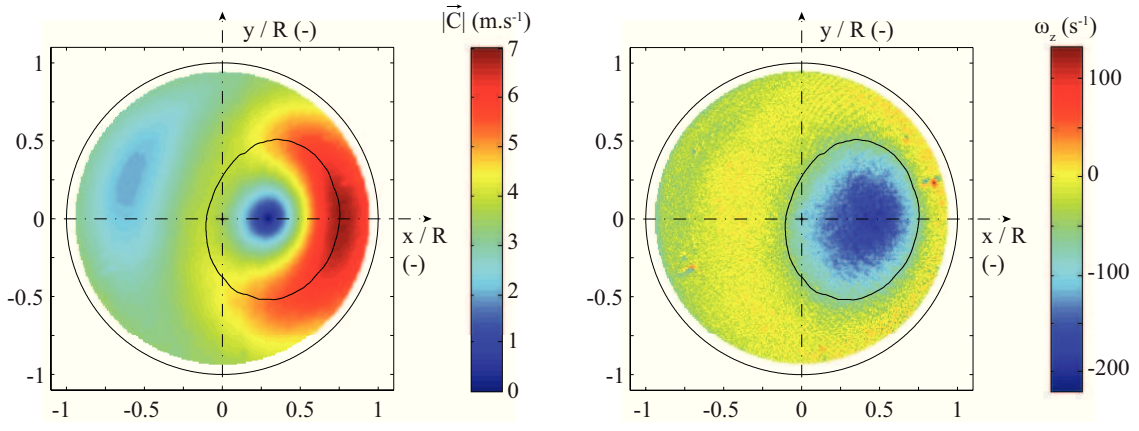

Figure 7: Velocity magnitude and vorticity for a given phase of the precession cycle in the PIV measurement section 3. The limits of the vortex core are indicated by the solid black contour ($Q_{\mathrm{ED}}/Q^*_{\mathrm{ED}} = 0.64$).

The limits of the vortex core must be defined properly. For this purpose, a second algorithm proposed by Graftieaux et al. [17] for the detection of the boundaries of large vortical structures is used. They introduced a second scalar γ_2, which is defined at a given point P by:

$$\gamma_2(P) = \frac{1}{N} \sum_{S} \frac{(\vec{PM} \wedge (\vec{C}(M) - \vec{C}(P))) \cdot \vec{z}}{\|\vec{PM}\| \cdot \|\vec{C}(M) - \vec{C}(P)\|} \tag{3}$$

with $\vec{C}(P)$ the average velocity vector within the domain S. Graftieaux et al. [17] showed that when the scalar $|\gamma_2|$ is greater than $2/\pi$, the flow is locally dominated by the rotating motion, which corresponds to the vortex core. An example of the phase averaged velocity field magnitude, together with the corresponding vorticity distribution, is presented in Figure 7. The boundaries of the vortex core are given by the black solid lines.

4. Results

4.1. Phase averaged velocity fields and vortex circulation

The magnitude of the phase averaged velocity fields obtained in the measurement section 3 is presented in Figure 8 for a given phase of the precession cycle.

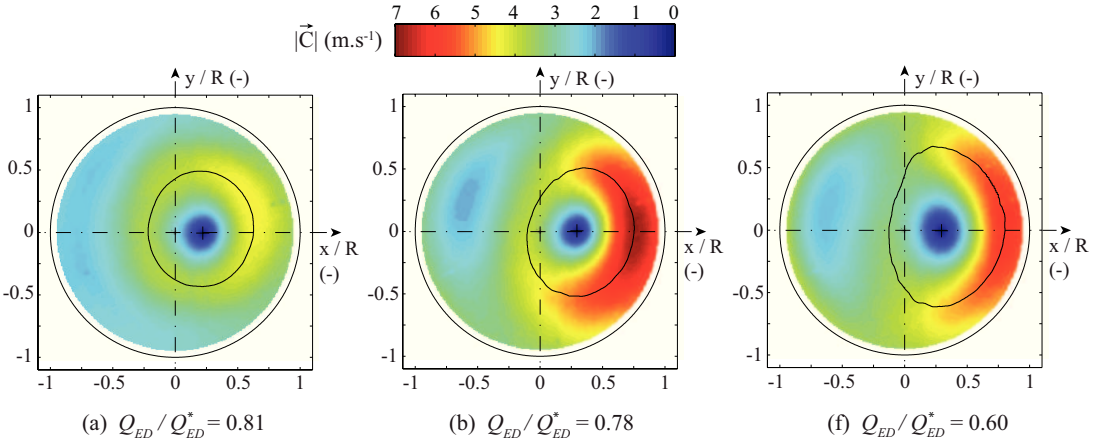

Figure 8: Influence of the discharge factor on the magnitude of the velocity fields in the measurement section 3. The black solid lines correspond to the limits of the vortex core.

For all the investigated values of the discharge factor, a large vortical structure is identified, corresponding to the precessing vortex core. The surface delimited by the solid black lines corresponds to the vortex core. However, a decrease in the value of the discharge factor modifies the structure of the vortex core. For the highest value of discharge factor, the vortex core is quasi-circular and the distribution of tangential velocity around the vortex centre is nearly axi-symmetric, whereas a slight acceleration of the flow between the vortex centre and the cone wall is already observed. By decreasing the value of the discharge factor, the vortex core takes an elliptical shape and the distribution of tangential velocity is increasingly asymmetric.

The values of the vortex circulation obtained for the operating points 1 and 2 are given in Table 2. In all the measurement sections, the vortex circulation strongly increases as the discharge factor is decreased, as it induces an increase of the swirl degree of the flow feeding the draft tube. For the operating point 3, it is not possible anymore to compute the vortex circulation as the identification of the vortex core limits fails for certain phases of the precession cycle.

Table 2: Value of the vortex circulation

Section	OP	Γ $(\mathrm{m^2\,s^{-1}})$
1	1	2.411
	2	3.026
2	1	2.211
	2	2.755
3	1	2.165
	2	2.881

4.2. Average trajectory and dispersion of the vortex centre

For each operating point, the vortex centre is identified for all the phase averaged velocity fields, enabling the reconstruction of the average vortex centre trajectory over one typical precession period. The results are presented in Figure 9 for the measurement sections 1, 2 and 3.

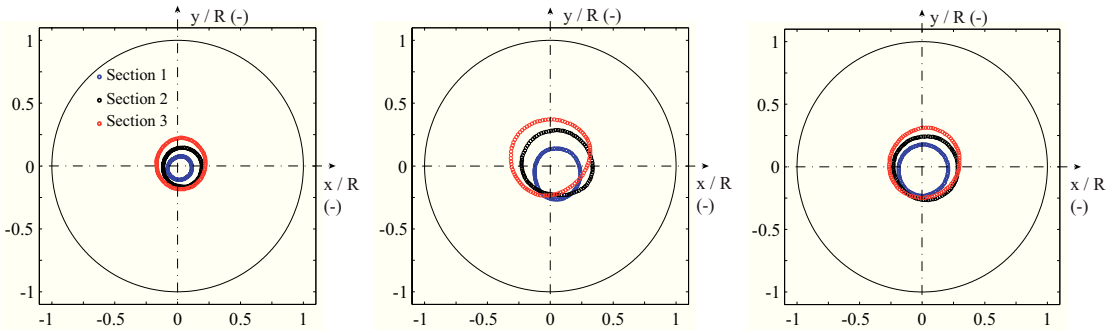

(a) $Q_{ED}/Q^*_{ED} = 0.81$ (b) $Q_{ED}/Q^*_{ED} = 0.64$ (c) $Q_{ED}/Q^*_{ED} = 0.60$

Figure 9: Trajectory of the vortex centre over one typical precession cycle for three values of the discharge factor.

The vortex trajectory features a strong asymmetry, which is increasingly pronounced as the discharge factor is decreased from the value $Q_{\mathrm{ED}}/Q^*_{\mathrm{ED}} = 0.81$ to the value $Q_{\mathrm{ED}}/Q^*_{\mathrm{ED}} = 0.64$. Moreover, the precession of the vortex experiences a strong widening of its trajectory. Below the transition from the flow regimes 2 to 3, the diameter of the vortex trajectory is however reduced and its asymmetry is less pronounced.

The instantaneous positions of the vortex centre present a dispersion around its average trajectory. The standard deviation of the vortex centre coordinates (x_c, y_c) is plotted as a function of the discharge factor in Figure 10. The standard deviation for both coordinates remains nearly constant within the flow regimes 1 and 2 and is comprised between 6 and 7 % of the section radius. Beyond the transition between the flow regimes 2 and 3, it however drastically increases, which is another evidence of the loss of periodicity and coherence in the vortex dynamics occurring for values of discharge factor $Q_{\mathrm{ED}}/Q^*_{\mathrm{ED}} < 0.62$.

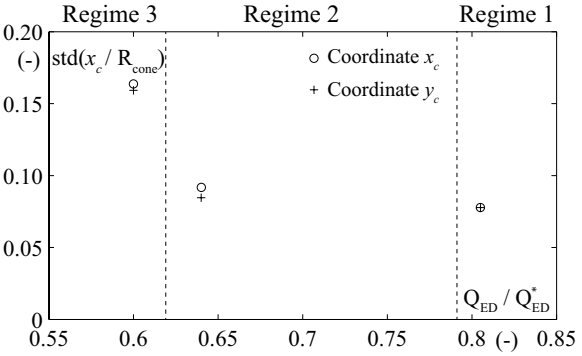

Figure 10: Standard deviation of the vortex centre coordinates (x_c, y_c) as a function of the discharge factor in the PIV measurement section 3.

5. Conclusion

The flow velocity fields are investigated in three horizontal cross-sections of a Francis turbine draft tube cone at part load operating conditions by means of PIV. The investigation is focused on three different values of the discharge factor in cavitation-free conditions. Furthermore, pressure fluctuations measurements are performed in a wide range of value of the discharge factor at different locations of the test-rig, including the draft tube cone and the upstream pipe of the machine. A methodology is proposed to recover properly by phase averaging the evolution of the velocity fields over one typical precession period. Based on the latter, the parameters of the vortex, such as trajectory and circulation, are determined for each operating point.

The results suggest the occurrence of three different flow regimes, depending on the value of the discharge factor. The vortex circulation and the diameter of the vortex trajectory reach their maximum value within the flow regime 2, for which the coherence of the pressure fluctuations measured in the cone is at its highest level. As a result, the amplitude of the pressure fluctuations measured in the upstream pipe of the machine is at its maximum. Beyond the transition from the regimes 2 to 3, an abrupt change in the vortex dynamics is observed, characterized by a retraction of its trajectory and a loss of coherence and periodicity. It is notably illustrated by an important increase of the dispersion of the instantaneous vortex centres around the average trajectory.

Acknowledgments

The research leading to the results published in this paper is part of the HYPERBOLE research project, granted by the European Commission (ERC/FP7- ENERGY-2013-1-Grant 608532). The authors would also like to thank BC Hydro for making available the reduced scale model, in particular Danny Burggraeve and Jacob Iosfin. Moreover, the authors would like to acknowledge the commitment of the Laboratory for Hydraulic Machines' technical staff, especially Georges Crittin, Maxime Raton, Alain Renaud and Vincent Berruex.

References

[1] Nishi M, Matsunaga S and Kubota T S Y 1982 Flow regimes in an elbow-type draft tube *Proceedings of the 11th IAHR Symposium on Hydraulic Machinery and Systems, Amsterdam, Netherlands*
[2] Dörfler P and Ruchonnet N 2012 *IOP Conference Series: Earth and Environmental Science* **15**
[3] Duparchy A, Guillozet J, De Colombel T and Bornard L 2014 *IOP Conference Series: Earth and Environmental Science* **22**
[4] Dörfler P 1982 System dynamics of the Francis turbine half load surge *Proceedings of the 11th IAHR Symposium on Operating Problem of Pump Stations and Powerplants, Amsterdam, Netherlands*
[5] Rheingans W 1940 *Transactions of the ASME* **62** 171–184
[6] Couston M and Philibert R 1998 *The International Journal on Hydropower and Dams* **1** 146–158

[7] Nicolet C, Herou J, Greiveldinger B, Allenbach P, Simond J and Avellan F 2006 Methodology for risk assessment of part load resonance in francis turbine power plant *Proceedings of the 1st IAHR Workgroup on Cavitation and Dynamics Problems in Hydraulic Machinery and Systems, Barcelona, Spain*
[8] Alligné S, Nicolet C, Tsujimoto Y and Avellan F 2014 *Journal of Hydraulic Research* **52**(3)
[9] Brennen C and Acosta A 1976 *Journal of Fluids Engineering, Transactions of the ASME* **98 Ser 1**(2) 182–191
[10] Landry C 2015 *Hydroacoustic Modeling of a Cavitation Vortex Rope for a Francis Turbine* Ph.D. thesis EPFL Lausanne, Switzerland
[11] Landry C, Favrel A, Müller A, Nicolet C and Avellan F 2016 *Journal of Hydraulic Research* (article in press)
[12] Iliescu M, Ciocan G and Avellan F 2008 *Journal of Fluids Engineering, Transactions of the ASME* **130**(2)
[13] Iliescu M, Houde S, Lemay S, Fraser R and Deschênes C 2011 Investigation of the cavitational behavior of an axial hydraulic turbine operating at partial discharge by 3D-PIV *Proceedings of the 9th International Symposium on Particle Image Velocimetry, Kobe, Japan, July*
[14] Müller A, Dreyer M, Andreini N and Avellan F 2013 *Experiments in Fluids* **54**(4)
[15] Favrel A, Müller A, Landry C, Yamamoto K and Avellan F 2015 *Experiments in Fluids* **56**(12)
[16] Müller A, Yamamoto K, Alligné S, Yonezawa K, Tsujimoto Y and Avellan F 2015 *ASME J. Fluids Eng.* **138**(2)
[17] Graftieaux L, Michard M and Nathalie G 2001 *Measurement Science and Technology* **12**(9)
[18] Dreyer M, Decaix J, Münch-Alligné C and Farhat M 2014 *Experiments in Fluids* **55**(11)